The 2021 outburst of RS Oph: a pictorial atlas of the spectroscopic evolution. II. From day 19 to 102 (solar conjunction)

Ulisse Munari[1] and Paolo Valisa[2]

1: INAF National Institute of Astrophysics, 36012 Asiago, Italy
2: ANS Collaboration, c/o Astronomical Observatory, 36012 Asiago, Italy

Abstract. We present the second part of our atlas of the spectral evolution of RS Oph during the 2021 nova outburst, characterized by a tight-monitoring in high-resolution with Echelle spectrographs mounted on the Varese 0.84m and Asiago 1.82m telescopes. In this Paper II we cover from day 19 to 102 (Aug 28 to Nov 19), the interval going from appearance of high ionization lines to the stop imposed on observations by the Solar conjunction. A third and final paper will map the spectral evolution after emersion from Solar conjunction (Jan 16, 2022) and up to the re-establishment of pre-outburst appearance, marking the spectroscopic end of the outburst. Some quick conclusions can be drawn from the data presented in this second part of our atlas:
(1) the spectra evolution has progressed in a smooth and gradual way, suggesting that both the expansion of the ejecta through the pre-existing RG wind and the photo-ionization from the central source did not encountered sudden discontinuities prior to switch-off of the nuclear burning;
(2) the 2021 spectral evolution is similar to that of the 2006 eruption (the latter much less accurately mapped), with a mirror-appearance of the triple-peaked line profiles (blue peak brighter than red in 2006, the opposite in 2021) probably related to the two outbursts occurring at opposite sides of the binary orbit followed by the red giant and the white dwarf companion;
(3) the evolution of the triple-peaked profiles progressed similarly through different excitation and ionization degrees, arguing in favor of a geometrical origin, as in a bipolar outflow nested to an equatorial torus; a discontinuity occurred around day 30 (at the time when the coronal lines were rising to their maximum), when the rate of shrinking in the velocity separation of the red and blue peaks dropped from -10 to -1 km s^{-1} per day;
(4) the time-behavior of coronal emission lines appears quite smooth, both in terms of radiated flux as well as evolution of the triple-peaked profiles, with a plateau at maximum lasting up to about day 87 (counted from maximum brightness), and the rise/decline times in agreement with progressive clearing of the ejecta and then cooling of the WD following switch-off of the nuclear burning;
(5) there seems to exist within RS Oph two distinct types of ejecta: (1) fast moving ones giving rise to Gaussian-like line profiles (primarely [NII] and [OIII]), that keep expanding at FWHM=1000 km s^{-1} with no sign of ongoing deceleration during the two months leading up to Solar conjunction, and (2) slower moving ejecta giving rise to the triple-peaked line profiles (HeI, HeII, coronal lines, and also Balmer lines at later times), for which the separation in velocity of blue and red peaks is still shrinking at the time of Solar conjunction when it reaches an average 330 km s^{-1};
(6) the "symbiotic band" at 6825 Å, due to Lyman scattering of OVI 1032 Å by neutral hydrogen, appears simultaneously with the coronal lines and evolves in parallel with them in terms of integrated flux: its very presence indicates that a sizeable part of the wind of the red giant was neutral while coronal lines were developing. In symbiotic stars in quiescence the 6825 Å band is normally observed only in systems undergoing stable nuclear burning, a condition that appears holding for RS Oph up to around day +87.

1. INTRODUCTION

This is the second of a three-parts atlas of the spectral evolution of the symbiotic and recurrent nova RS Oph during its 2021 outburst. The first part (Munari and Valisa 2021c, hereafter Paper I) covered the initial phase of the evolution up to emersion of high ionization emission lines, corresponding to interval 0 to 18 days past optical maximum (Aug 9 to 27, 2021). The present Paper II goes from day 19 to 102 (Aug 28 to Nov 19, 2021), when a stop was imposed on observations by Solar conjunction. A third and final paper will deal with the period going from emersion from Solar conjunction (we resumed observations of RS Oph in the pre-dawn sky on January 16, 2022; Munari and Valisa 2022) up to the re-establishment of pre-outburst brightness (currently dropped below that level as in all previous outbursts at similar phases) and of pre-outburst spectral appearance.

The amount of information stored in a ~daily spectral monitoring in high-resolution/high-SN/absolute-fluxes of the current outburst of RS Oph is just immense, and will take a long time and a great effort to be (at least in part) digested. Nonetheless, there is a certain urgency to present at least a quick overlook (and without much discussion) of some basic characteristics of such spectral evolution, in support of investigations at wavelengths other then optical.

A relevant feature of our atlas is in the great homogeneity maintained through the whole observing campaign: just three and the same spectrographs on meter-class telescopes (Asiago 1.22m and 1.82m, Varese 0.84m; all located on the Italian Alps), identical IRAF-based data reduction and calibration procedures (as described in the book by Zwitter and Munari 2000), same set of spectrophotometric standards adopted at all three telescopes, etc.

Following on the style of Paper I, a series of 3200-8000 Å spectra at selected dates are presented to document the overall appearance and evolution at optical wavelengths, and then the focus shifts to selected emission lines for which the absolutely-fluxed profiles are presented at 42 distinct dates distributed over the day 19-to-102 time interval. A few key plots than follow, presenting: a comparison of lines profiles for the 2006 and 2021 outbursts; the shrinking with time of the separation in velocity of triple-peaked lines; the evolution in the integrated flux of some lines and of the underlying true continuum away from lines; the behavior with time of the FWHM of emission lines; and the evolution of the integrated flux of iron coronal lines [FeX], [FeXI], [FeXIV] and for reference of [FeVII], as well as the Lyman scattering at 6825 Å of OVI 1032 Å by neutral hydrogen.

2. RS OPH

The current outburst has triggered observations of RS Oph over the whole electromagnetic spectrum. As noted in Paper I, preliminary reports have been presented by Cheung et al. (2021a,b) and Wagner & HESS Collaboration (2021a,b) for γ-rays; Enoto et al. (2021a,b), Ferrigno et al. (2021), Luna et al. (2021), Page (2021a), Page et al. (2021), Rout et al. (2021) and Shidatsu et al. (2021) for the X-rays; Mikolajewska et al. (2021), Munari & Valisa P (2021a,b), Shore et al. (2021a,b,c), and Taguchi et al. (2021a,b) for the optical; Woodward et al. (2021a) for the infrared; and Sokolovsky et al. (2021) and Williams et al. (2021) for the radio. The results of the search for neutrino emission has been given by Pizzuto et al. (2021), and on the polarization of optical light by Nikolov & Luna (2021).

Following the release of Paper I, Page (2021b) announced RS Oph entering the super-soft X-ray emission phase as later confirmed by Pei et al. (2021) and Orio et al. (2021b,c), with description of X-ray grating spectra given by Orio et al. (2021a). Montez et al. (2021) reported on the detection and analysis of extended bipolar X-ray emission stemming from the 2006 eruption. Detection of very-high-energy gamma rays from RS Oph have been reported and analyzed in conjunction with Fermi-LAT data by the H.E.S.S. Collaboration (2022) and MAGIC Collaboration (2022). Zamanov et al. (2021a) noted the disappearance of flickering and some optical photometry was provided by Ricra et al. (2021), while Fajrin et al. (2021) reported about their spectroscopic monitoring of Hα as also Zamanov et al. (2021b) did. Emersion of coronal emission lines in optical spectra was first reported by Munari et al. (2021), followed by a similar detection at infrared wavelengths by Woodward et al. (2021). Finally, the photometric and spectroscopic status of RS Oph after emersion in mid January 2022 from Solar conjunction has been described by Munari et al. (2022).

3. OBSERVATIONS

We have used the same telescopes/spectrographs and data acquisition/reduction procedures as in Paper I.

Echelle observations have been recorded with (1) the 1.82m telescope + REOSC Echelle spectrograph operated in Asiago by the National Institute of Astrophysics INAF, that covers in 32 orders and at 22,000 resolving power (for the usual 1.8-arcsec slit width) the wavelength range 3500-7350 Å, without inter-order gaps; and (2) the Varese 0.84m telescope operated by ANS Collaboration and equipped with an Astrolight Inst. mk.III Multi-Mode spectrograph, that in the Echelle configuration covers the 4250-8900 Å range at a 18,000 resolving power (for a 2-arcsec slit) and without inter-order gaps.

Low resolution observations have been acquired with the B&C spectrograph on the 1.22m telescope operated in Asiago by the University of Padova. It offers a great sensitivity at near-UV wavelengths, and spectra obtained with the 300 ln/mm grating blazed at 5000 Å allows to cover the 3200-8000 Å range at 2.3 Å/pix dispersion. The observations here presented at been recorded at FWHM(PSF)=2 pix sampling.

Data reduction at all three telescopes has been performed in IRAF and has included all usual steps of correction for bias, dark and flat, sky subtraction, wavelength calibration, and heliocentric correction. Spectrophotometric standards, located close on the sky to RS Oph, have been observed each night soon before and/or after the RS Oph to achieve an optimal flux calibration, which was also essential to accurately merge the individual 30 Echelle orders into a single 1D fluxed spectrum without the usual dents at the points of junction.

Journals of observations for Echelle and B&C spectra are provided in Tables 1 and 2, where the elapsed time $t - t_{\rm max}$ is computed from maximum optical brightness taken from Paper 1 to have occurred on

$$t^{V}_{\rm max} = 2459436.18 \text{ JD} \quad \text{2021 Aug 09.68} \quad (\pm 0.05) \tag{1}$$

Table 1: Journal of Echelle spectroscopic observations obtained with the Varese 0.84m and Asiago 1.82m telescopes.

date	HJD	t-t_{max}	expt (sec)	tel.	date	HJD	t-t_{max}	expt (sec)	tel.
2021-08-09	2459436.300	0.12	540	0.84m	2021-09-07	2459465.312	29.13	5400	0.84m
2021-08-09	2459436.337	0.16	540	0.84m	2021-09-08	2459466.281	30.10	3000	0.84m
2021-08-09	2459436.373	0.19	540	0.84m	2021-09-09	2459467.322	31.14	2700	0.84m
2021-08-09	2459436.404	0.22	720	0.84m	2021-09-10	2459468.308	32.13	4200	0.84m
2021-08-10	2459437.320	1.14	720	0.84m	2021-09-11	2459469.285	33.11	2430	0.84m
2021-08-10	2459437.389	1.21	720	0.84m	2021-09-12	2459470.268	34.09	2700	0.84m
2021-08-11	2459438.342	2.16	1440	0.84m	2021-09-13	2459471.271	35.09	3000	0.84m
2021-08-12	2459439.332	3.15	1200	0.84m	2021-09-14	2459472.290	36.11	3600	0.84m
2021-08-13	2459440.308	4.13	900	0.84m	2021-09-17	2459475.277	39.10	4200	0.84m
2021-08-14	2459441.367	5.19	1440	0.84m	2021-09-21	2459479.297	43.12	3000	0.84m
2021-08-15	2459442.310	6.13	1200	0.84m	2021-09-24	2459482.269	46.09	3000	0.84m
2021-08-16	2459443.324	7.14	3000	0.84m	2021-09-27	2459485.282	49.10	4050	0.84m
2021-08-17	2459444.306	8.13	900	0.84m	2021-09-29	2459487.246	51.07	4050	0.84m
2021-08-18	2459445.310	9.13	1500	0.84m	2021-10-01	2459489.242	53.06	4050	0.84m
2021-08-19	2459446.299	10.12	240	1.82m	2021-10-06	2459494.240	58.06	4800	0.84m
2021-08-19	2459446.353	10.17	1500	0.84m	2021-10-08	2459496.235	60.05	4800	0.84m
2021-08-20	2459447.308	11.13	1500	0.84m	2021-10-10	2459498.230	62.05	3150	0.84m
2021-08-21	2459448.301	12.12	1500	0.84m	2021-10-12	2459500.231	64.05	4800	0.84m
2021-08-22	2459449.296	13.12	1500	0.84m	2021-10-15	2459503.235	67.06	3600	0.84m
2021-08-22	2459449.297	13.12	540	1.82m	2021-10-17	2459505.225	69.04	3600	0.84m
2021-08-23	2459450.294	14.11	2400	0.84m	2021-10-19	2459507.222	71.04	4050	0.84m
2021-08-24	2459451.314	15.13	1800	0.84m	2021-10-22	2459510.217	74.03	900	1.82m
2021-08-25	2459452.296	16.12	1800	0.84m	2021-10-23	2459511.218	75.04	4050	0.84m
2021-08-25	2459452.312	16.13	540	1.82m	2021-10-26	2459514.223	78.04	4800	0.84m
2021-08-26	2459453.285	17.11	2400	0.84m	2021-10-28	2459516.218	80.04	4050	0.84m
2021-08-27	2459454.309	18.13	600	0.84m	2021-11-01	2459520.234	84.05	4800	0.84m
2021-08-28	2459455.302	19.12	2100	0.84m	2021-11-04	2459523.209	87.03	4200	0.84m
2021-08-29	2459456.292	20.11	2400	0.84m	2021-11-05	2459524.210	88.03	4200	0.84m
2021-08-30	2459457.366	21.19	3600	0.84m	2021-11-07	2459526.210	90.03	4500	0.84m
2021-08-31	2459458.280	22.10	2400	0.84m	2021-11-11	2459530.209	94.03	3600	0.84m
2021-09-01	2459459.287	23.11	2100	0.84m	2021-11-12	2459531.209	95.03	2700	0.84m
2021-09-02	2459460.274	24.09	1500	0.84m	2021-11-18	2459537.214	101.03	2700	0.84m
2021-09-03	2459461.289	25.11	3000	0.84m	2021-11-19	2459538.204	102.02	2700	0.84m
2021-09-06	2459464.314	28.13	4200	0.84m					

Table 2: Journal of B&C spectroscopic observations obtained with the Asiago 1.22m telescope.

date	HJD	t-t_{max}	expt (sec)	tel.	date	HJD	t-t_{max}	expt (sec)	tel.
2021-08-09	2459436.284	0.10	100	1.22m	2021-08-19	2459446.281	10.10	110	1.22m
2021-08-09	2459436.331	0.15	150	1.22m	2021-08-19	2459446.330	10.15	90	1.22m
2021-08-10	2459437.300	1.12	120	1.22m	2021-08-20	2459447.307	11.13	120	1.22m
2021-08-10	2459437.383	1.20	150	1.22m	2021-08-20	2459447.369	11.19	90	1.22m
2021-08-11	2459438.298	2.12	90	1.22m	2021-08-22	2459449.321	13.14	150	1.22m
2021-08-11	2459438.419	2.24	130	1.22m	2021-08-23	2459450.279	14.10	150	1.22m
2021-08-12	2459439.281	3.10	90	1.22m	2021-08-31	2459458.297	22.12	95	1.22m
2021-08-12	2459439.295	3.12	170	1.22m	2021-09-01	2459459.282	23.10	85	1.22m
2021-08-12	2459439.365	3.19	120	1.22m	2021-09-02	2459460.267	24.09	135	1.22m
2021-08-13	2459440.319	4.14	120	1.22m	2021-09-02	2459460.354	24.17	90	1.22m
2021-08-13	2459440.378	4.20	120	1.22m	2021-09-03	2459460.349	24.17	90	1.22m
2021-08-14	2459441.351	5.17	100	1.22m	2021-09-05	2459463.267	27.09	110	1.22m
2021-08-15	2459442.342	6.16	120	1.22m	2021-09-12	2459470.284	34.10	130	1.22m
2021-08-15	2459442.386	6.21	90	1.22m	2021-09-27	2459485.264	49.08	120	1.22m
2021-08-17	2459444.301	8.12	120	1.22m	2021-10-16	2459504.233	68.05	900	1.22m
2021-08-18	2459445.309	9.13	120	1.22m	2021-11-11	2459530.201	94.02	1200	1.22m

4. OVERALL SPECTRAL APPEARANCE

The low-resolution spectra obtained with the Asiago 1.22m + B&C telescope allow to grasp an overall picture of the evolution of RS Oph during the 19 to 102 day interval under consideration in this Paper II. A selection of them is presented in Figure 1.

The brightness of the underlying continuum and the integrated flux of emission lines have both declined steadily, the latter at a lower pace so that - as in most novae - the contrast of emission lines appear to increase with time, expecialy for the nebular ones like [OIII], [OII], [OI], [NeIII], [NII], [SII], etc. Coronal emission lines started to emerge between days 25-30, and rapidly increased in intensity with [FeX] remaining always the strongest of all. The increase in ionization is well illustrated by the steady progress with time of the [NeV] 3427 / OIII ratio.

It is evident in Figure 1 how the region around 4770 Å has remained rather free from the presence of emission lines, and consequently it offers the possibility to evaluate there the flux level of the background continuum, at blue wavelengths where the direct emission from the stable red giant is expected to emerge at later times than in the red.

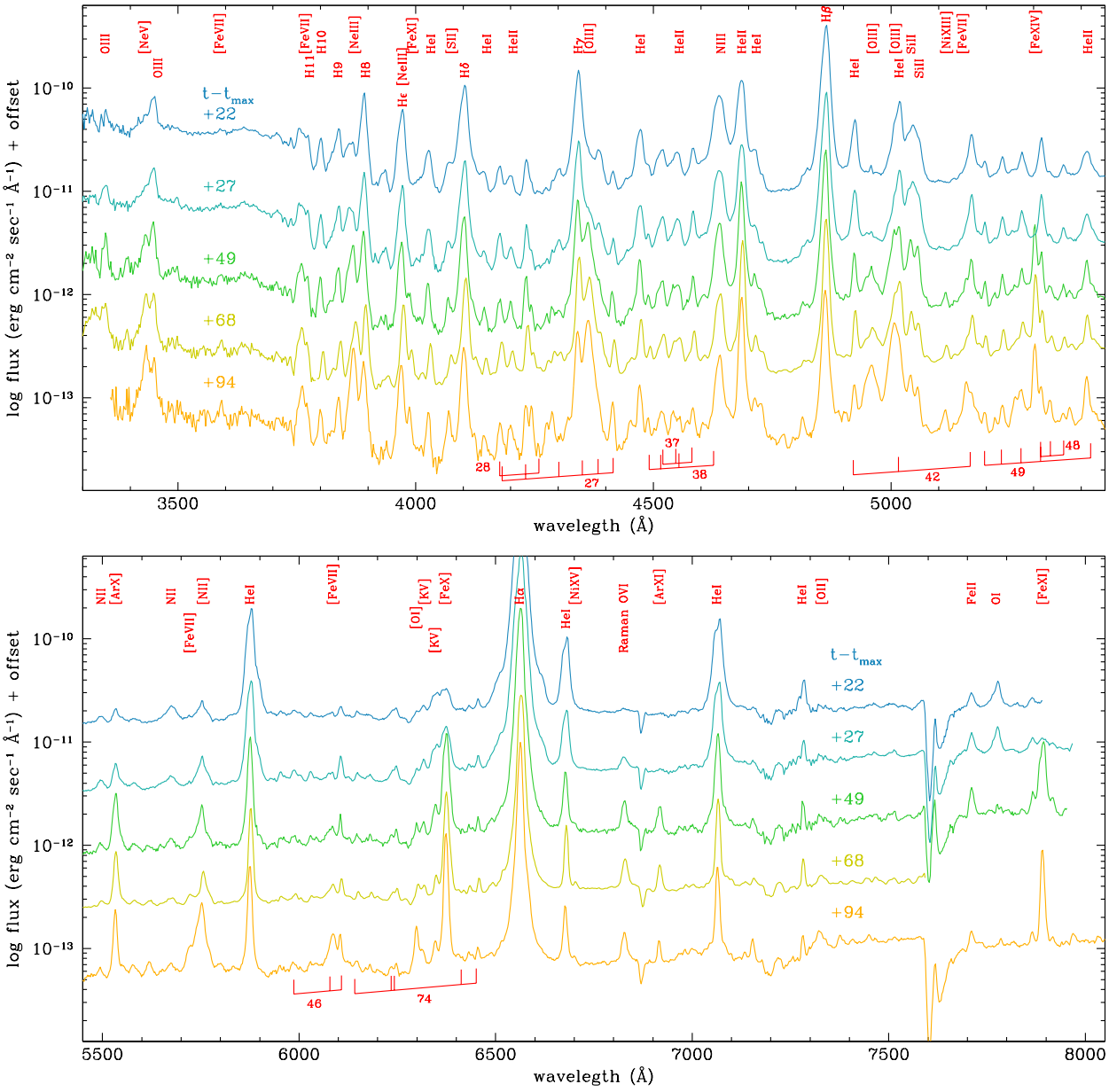

Figure 1: Sequence of Asiago 1.22m + B&C spectra highlighting the evolution of RS Oph during the 19 to 102 day interval. The most relevant emission lines are identified at the top, and the comb-markings at the bottom identified FeII multiplets. The observing epochs are marked as days passed since maximum brightness $t - t_{\max}$ (cf. Table 2).

4. COMPARISON OF 2006 ANS 2021 LINE PROFILES

As the photometric evolution of the current outburst is a close replica of what seen in 2006 (and previous ones), a marked similarity affects also the spectra, passing through similar phases at similar times. There is however a striking difference: the mirror appearance of tripled-peaked profiles, as illustrated in Figure 2. Throughout the 2006 event and for all lines presenting tripled-peaked profiles, the blue peak has always been brighter than the red peak: the exact contrary is observed for the 2021 outburst, with the blue peak stronger than the red one at all phases and for all lines as well illustrated by the time sequences of profiles presented in Figures 6 to 11. With all probability this difference relates to the fact the 2006 and 2021 outbursts occurred on opposite sides of the binary orbit.

The triple-peaked profile is present or at least recognizable in nearly all lines observed in 2021, with the exception of [NII], [OIII] and a few others. Also Balmer lines evolved to a triple-peaked profile by the time the Solar conjunction was approaching.

For all triple-peaked line profiles (cf HeI, HeII, or coronal lines in Figures 6 to 10), the side peaks (i.e. the red and the blue peak) decline faster than the central peak. At late times, for some of the riple-peaked lines (eg. [FeXIV] 5303) only the central peak remained visible.

Balmer lines presented a lower degree of "mirror symmetry" when comparing 2006 and 2021 profiles. From Figure 2, a triple-peaked profile seems present in Hβ in 2006 already at day 30, but with a reversed blue/red peak ratio compared to the other 2006 lines and with a prominent central peak, while Hα looks rather symmetrical. With a certain degree of imagination, a tripled-peaked profile can be recognized also in the 2021 Hβ profile for day 30 in Figure 2 but, differently from 2006, with a insignificant central peak and a blue/red peak ratio similar to that of the other lines and not reversed.

When comparing the relative displacement of the narrow (from the ionized wind) and very broad (from expanding ejecta) components in the [NII] 5755 profile, a "mirror symmetry" is present for them too when comparing 2006 to 2021 profiles in Figure 2.

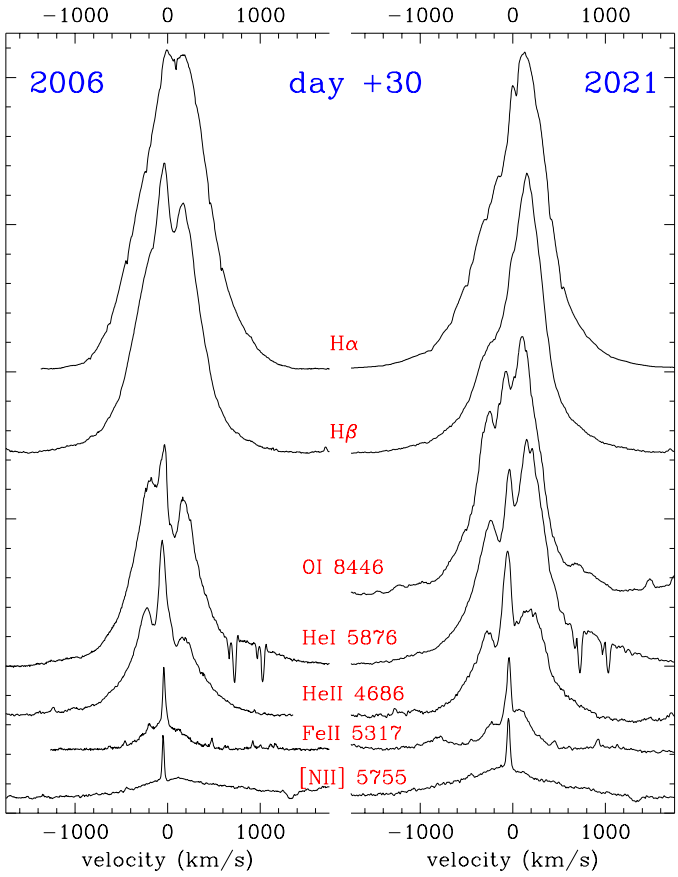

Figure 2: A comparison of the profile of a few representative lines, at day +30 from optical maximum, for the 2006 (from Munari et al. 2007) and 2021 outbursts.

5. VELOCITY SEPARATION OF TRIPLE-PEAKED LINE PROFILES

The velocity separation (ΔV) of red and blue peaks has been measured on the Echelle spectra of Figures 6 to 11 for a number of emission lines and its progression with time is plotted in Figure 3.

Higher ionization lines as HeII, [FeX] and [FeXIV] behave all rather similarly, with a separation ~60 km s^{-1} larger than for lower excitation lines like FeII and OI. The HeI lines locate neatly in between, with the green line in Figure 3 being a spline fitting to all measurable HeI lines, in particular to 6678 and 5015 singlet lines, and 5876 and 7065 triplet lines.

The behavior of ΔV for HeI lines (copied by HeII) is characterized by a marked change in slope taking place during the day 30 to 50 interval (this is the same time interval over which coronal lines reach in turn their respective plateau maxima, from [FeX] around day 30 to [FeXIV] about day 50; see Figure sect. 7 and Figure 5 below): namely, before day 30 ΔV steadily reduces by −10 km s^{-1} each day, while after day 50 such shrinking is drastically slowed to a mere −1 km s^{-1} per day.

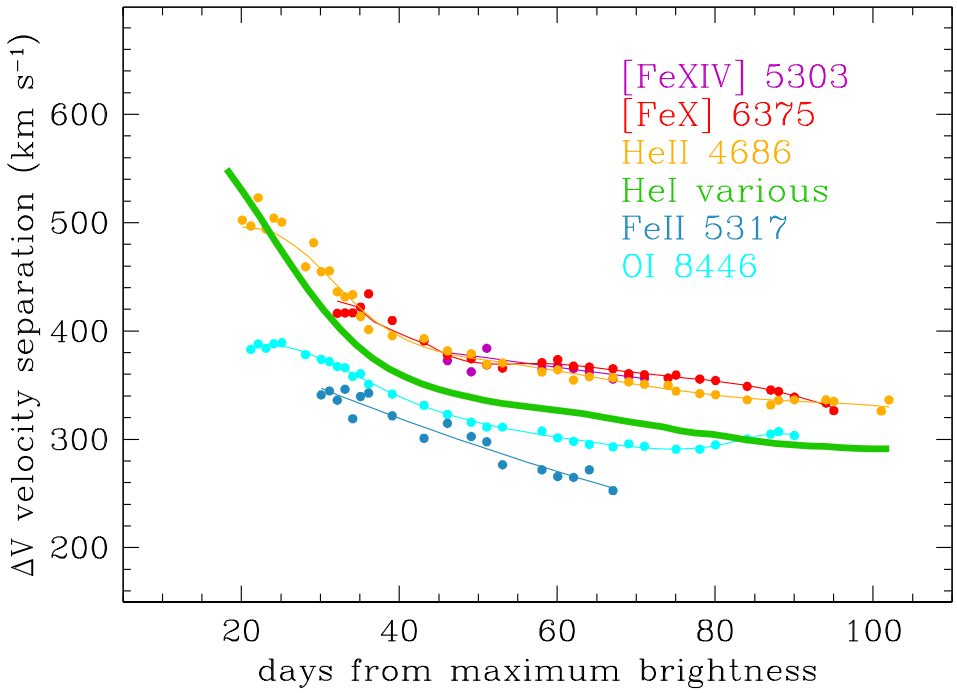

Figure 3: Velocity separation of the blue and red peaks of the triple-peaked profiles for selected lines on the 2021 Echelle spectra of RS Oph presented in Figures 6 to 11. By "HeI various" we mean a spline fitting to all measurable HeI lines, in particular the 6678 and 5015 singlet lines, and 5876 and 7065 triplet lines.

6. EVOLUTION OF INTEGRATED FLUX AND WIDTH OF BALMER LINES

The evolution in terms of integrated flux of Hα and Hβ emission lines is presented in the top panel of Figure 4, compared to the background brightness measured at 4770 Å. The decline in flux of Hα and Hβ has been very smooth and very similar, with measurement of initial Hα values being probably affected by the glare of the flash-ionized wind of the red-giant. A marked acceleration of the decline in flux sets around day +85, contemporaneous with the coronal lines abandoning the plateau maximum and beginning their rapid descent (cf. next section and Figure 5). The change in slope of Hα and Hβ has been somewhat mirrored by a similar change visible for the intensity of the background measured at 4770 Å. At early times the flux in the continuum declines must faster that flux in the Balmer lines, and only after day 30 they behave in parallel. The fluxes for 4770 Å and Hβ are tabulated in Table 3.

The evolution of the width of Hα and Hβ emission lines is illustrated in the bottom panel of Figure 4. Both behave very smoothly and rather similarly, with differences at latest epochs being probably spurious and induced by the appearance of the triple-peaked profile occuring first in Hγ, then Hβ, and only last in Hα.

From the bottom panel of Figure 4 it is evident how the width of all lines displaying, sooner or later, a triple-peaked profile ended converging toward FWHM≈330 km s^{-1}, a value than was still shrinking at the time when Solar

conjunction put a stop to the observations. On the contrary, emission lines like [NII] and [OIII] showing a profile characterized by a single broad Gaussian (ignoring the superimposed sharp peak originating in the quiet and flashed wind of the red giant), had already reached their terminal width at much earlier times (day ~45), with no further significantive shrinking afterward. Their terminal width, FWHM≈1000 km s^{-1}, is three times broader than for triple-peaked profiles.

It seem that within RS Oph co-existed two distinct types of ejecta: (1) a faster moving one, giving rise to the Gaussian-like broad profiles for [NII] and [OIII], leaving the central binary in a sort of spherical arrangement at a terminal ~425 km s^{-1} velocity (taking it as FWHM/2*sqrt*2 ln 2); and (2) a slower moving one, giving rise to the triple-peaked profiles, with the material confined in the bipolar regions moving away at ~165 km s^{-1} from the material originating the central peak and at rest with the barycenter of the binary.

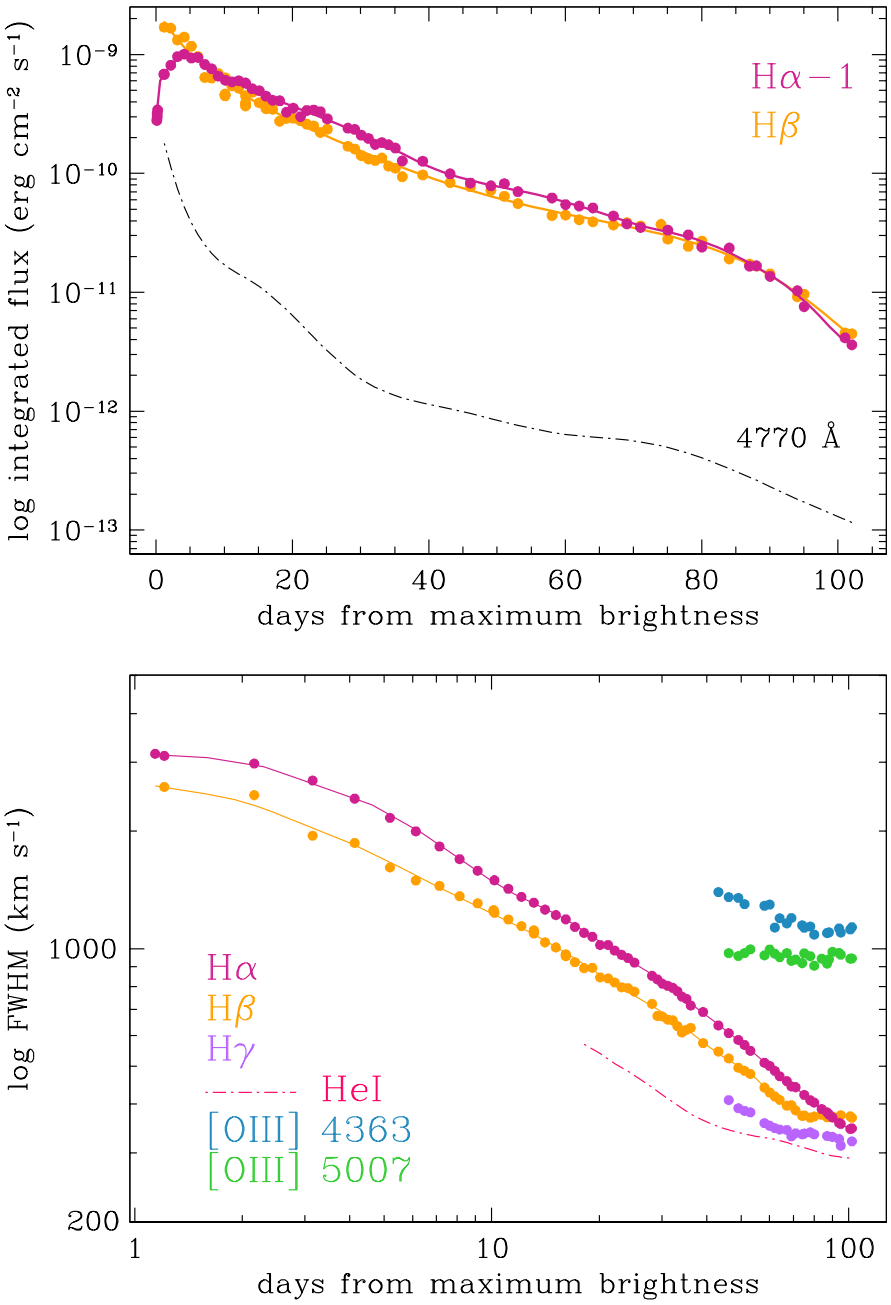

Figure 4: *Top panel*: evolution of the integrated flux of Hα and Hβ emission lines (log scale), measured on the 2021 Echelle spectra of RS Oph presented in Figures 6 to 11. Note the "−1" shift for Hα in the top panel, for an easier comparison with Hβ. For comparison, the dot-dashed line is the flux in the background continuum measured at 4770 Å (expressed as erg cm^{-2} s^{-1} Å^{-1}). *Bottom panel*: evolution of the FWHM of Hα and Hβ emission lines (log-log plot). Measurements for [OIII] 4363 are reported for epochs when it can be measured sufficiently clean from interference by nearby Hγ. The dot-dashed line is the "HeI various" from previous Figure 3 (cf. sect.5).

7. EVOLUTION OF CORONAL AND OVI EMISSION LINES

A hallmark of the 2021 and all previous outbursts of RS Oph is the development of strong coronal lines. We have measured the integrated flux of the iron coronal lines in the Echelle spectra of Figures 6 and 7, and tabulated them in Table 3 with a graphical presentation given in Figure 5. In the same figure, we have plotted for comparison the behavior of the continuum at 4770 Å and of the Lyman scattering by neutral hydrogen at 6825 Å of OVI 1032 (the "symbiotic bands" observed only in symbiotic stars undergoing nuclear burning at the surface of their white dwarfs).

The coronal lines started to appear with day 23, when the optical thickness of the expanding ejecta lowered sufficiently to allow ionizing photon to spread through. After a rapid rise in intensity, they all levelled off at a plateau maximum which was very smooth and that mildly declined in pace with the continuum background emission. Even if their appearance and their reaching maximum brightness happened in a succession paralleling their ionization degree, all the coronal lines left the plateau maximum at basically the same time, around day 87, to begin a rapid decline consistent with a switching off of the nuclear burning on the white dwarf of RS Oph.

Of special interest is the presence and behavior of the "symbiotic band" at 6825 Å. This band is observed in the symbiotic stars that in quiescence are powered by nuclear burning of the material accreted by their WDs. For a long time its origin has remained unidentified, until the mystery was solved by Schmid (1989) is terms of Lyman scattering at 6825 and 7088 Å of the ultraviolet doublet OVI 1036, 1036 Å by neutral hydrogen present within the binary. During the quiescence in between the outbursts, RS Oph does not burn on its WD and does not display the 6825 and 7088 Å bands (Munari and Zwitter 2002), which are observable only during nova outbursts (the 7088 Å band is much weaker than 6825 Å and essentially lost in the bright wings of HeI 7065). The behavior of 6825 Å in Figure 5 is rather similar to the coronal lines in terms of time of appearance, rising rate, plateau maximum, and onset of the decline. The very presence of 6825 Å proves that a sizeable fraction of the wind of the red giant was not ionized at the time the coronal lines reached their maximum emission; its long lasting plateau further supports the notion that nuclear burning was active up to the begin of the decline around days 85-90.

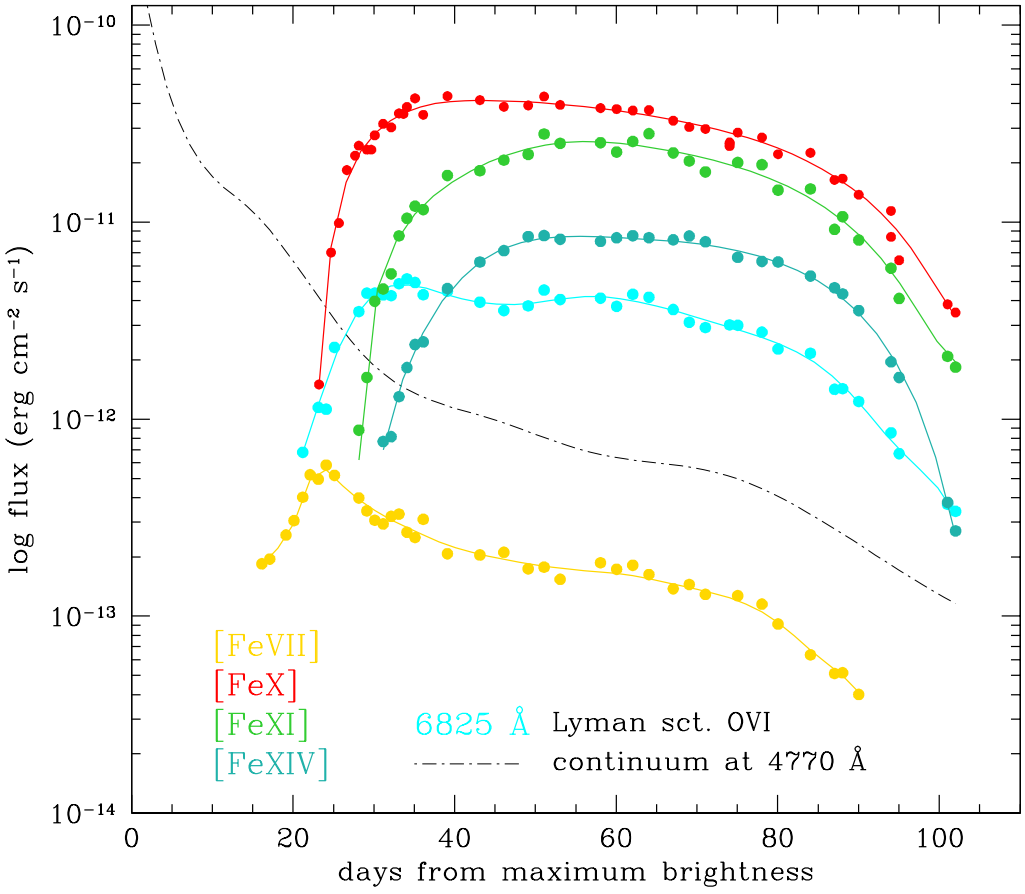

Figure 5: Evolution along the 2021 outburst of the integrated flux of coronal emission lines [FeX] 6375, [FeXI] 7892, and [FeXIV] 5303 Å, and for comparison also of [FeVII] 6087 Å, the "symbiotic band" at 6825 Å (Lyman scattering at 6825 Å of OVI 1302 by neutral hydrogen), and the continuum at 4770 Å (the latter expressed as erg cm^{-2} s^{-1} Å^{-1}).

Table 3: Logarithm of the flux in the continuum (in erg cm^{-2} s^{-1} Å^{-1}) and logarithm of the integrated flux (in erg cm^{-2} s^{-1}) of Hβ, [FeVII] 6087, [FeX] 6375, [FeXI] 7892, and [FeXIV] 5303 emission lines from the Echelle spectra listed in Table 1 and displayed in Figure 6 to 11.

t-t$_{max}$	4770 Å	Hβ	[FeVII]	[FeX]	[FeXI]	[FeXIV]
1.14	−9.731	−8.756				
1.21	−9.747	−8.770				
2.16	−9.951	−8.778				
3.15	−10.129	−8.878				
4.13	−10.280	−8.853				
5.19	−10.415	−8.930				
6.13	−10.514	−9.017				
7.14	−10.602	−9.193				
8.13	−10.671	−9.197				
9.13	−10.728	−9.160				
10.12	−10.773	−9.340				
10.17	−10.775	−9.196				
11.13	−10.812	−9.264				
12.12	−10.846	−9.283				
13.12	−10.879	−9.402				
14.11	−10.912	−9.318				
15.13	−10.952	−9.405				
16.13	−10.995	−9.443	−12.734			
17.11	−11.041	−9.461	−12.710			
19.12	−11.147	−9.537	−12.588			
20.11	−11.203	−9.535	−12.515			
21.19	−11.265	−9.556	−12.396			
22.10	−11.319	−9.586	−12.282			
23.11	−11.378	−9.601	−12.305	−11.824		
24.09	−11.435	−9.656	−12.234	−11.154		
25.11	−11.493	−9.628	−12.285	−11.005		
28.13	−11.649	−9.772	−12.400	−10.612	−12.056	
29.13	−11.693	−9.795	−12.465	−10.632	−11.789	
30.10	−11.731	−9.850	−12.513	−10.559	−11.402	
31.14	−11.768	−9.879	−12.532	−10.501	−11.339	−12.113
32.13	−11.798	−9.891	−12.493	−10.519	−11.262	−12.089
33.11	−11.825	−9.871	−12.482	−10.448	−11.070	−11.886
34.09	−11.849	−9.939	−12.574	−10.415	−10.980	−11.738
35.09	−11.870	−9.956	−12.601	−10.372	−10.919	−11.621
36.11	−11.889	−10.028	−12.508	−10.455	−10.936	−11.608
39.10	−11.933	−10.013	−12.683	−10.360	−10.763	−11.337
43.12	−11.981	−10.078	−12.690	−10.380	−10.739	−11.202
46.09	−12.020	−10.111	−12.676	−10.414	−10.685	−11.144
49.10	−12.064	−10.143	−12.760	−10.407	−10.656	−11.074
51.07	−12.093	−10.193	−12.751	−10.362	−10.553	−11.068
53.06	−12.121	−10.253	−12.813	−10.405	−10.600	−11.087
58.06	−12.180	−10.355	−12.729	−10.421	−10.597	−11.097
60.05	−12.196	−10.351	−12.762	−10.426	−10.644	−11.079
62.05	−12.208	−10.390	−12.742	−10.433	−10.590	−11.069
64.05	−12.218	−10.407	−12.789	−10.431	−10.551	−11.079
67.06	−12.232	−10.433	−12.861	−10.485	−10.648	−11.089
69.04	−12.243	−10.414	−12.840	−10.517	−10.690	−11.070
71.04	−12.258	−10.442	−12.889	−10.527	−10.745	−11.100
74.04	−12.290	−10.429	−12.906	−10.601	−10.711	−11.137
75.04	−12.303	−10.553	−12.896	−10.545	−10.697	−11.178
78.04	−12.353	−10.614	−12.939	−10.570	−10.708	−11.199
80.04	−12.392	−10.570	−13.040	−10.655	−10.837	−11.202
84.05	−12.482	−10.719	−13.196	−10.648	−10.831	−11.273
87.03	−12.556	−10.763	−13.291	−10.786	−11.037	−11.333
88.03	−12.582	−10.779	−13.288	−10.779	−10.972	−11.364
90.03	−12.635	−10.845	−13.398	−10.861	−11.091	−11.449
94.03	−12.741	−11.038		−11.074	−11.234	−11.709
95.03	−12.767	−11.016		−11.193	−11.387	−11.788
101.03	−12.913	−11.342		−11.417	−11.681	−12.423
102.02	−12.935	−11.349		−11.459	−11.736	−12.567

9. PICTORIAL EVOLUTION OF SELECTED EMISSION LINES

In Figures 6 to 11 we present the temporal evolution of a sample of emission lines from our Echelle spectra. The $t - t_{\rm max}$ time from maximum (in days) is marked in red next to each spectrum. The spectra are plotted in a log-flux scale + offset, which makes visible both faint features on the wings as well as the vastly brighter core. Earlier epochs are covered in Paper I, from which for continuity and overlap we take the first two spectra for day 16 and 17.

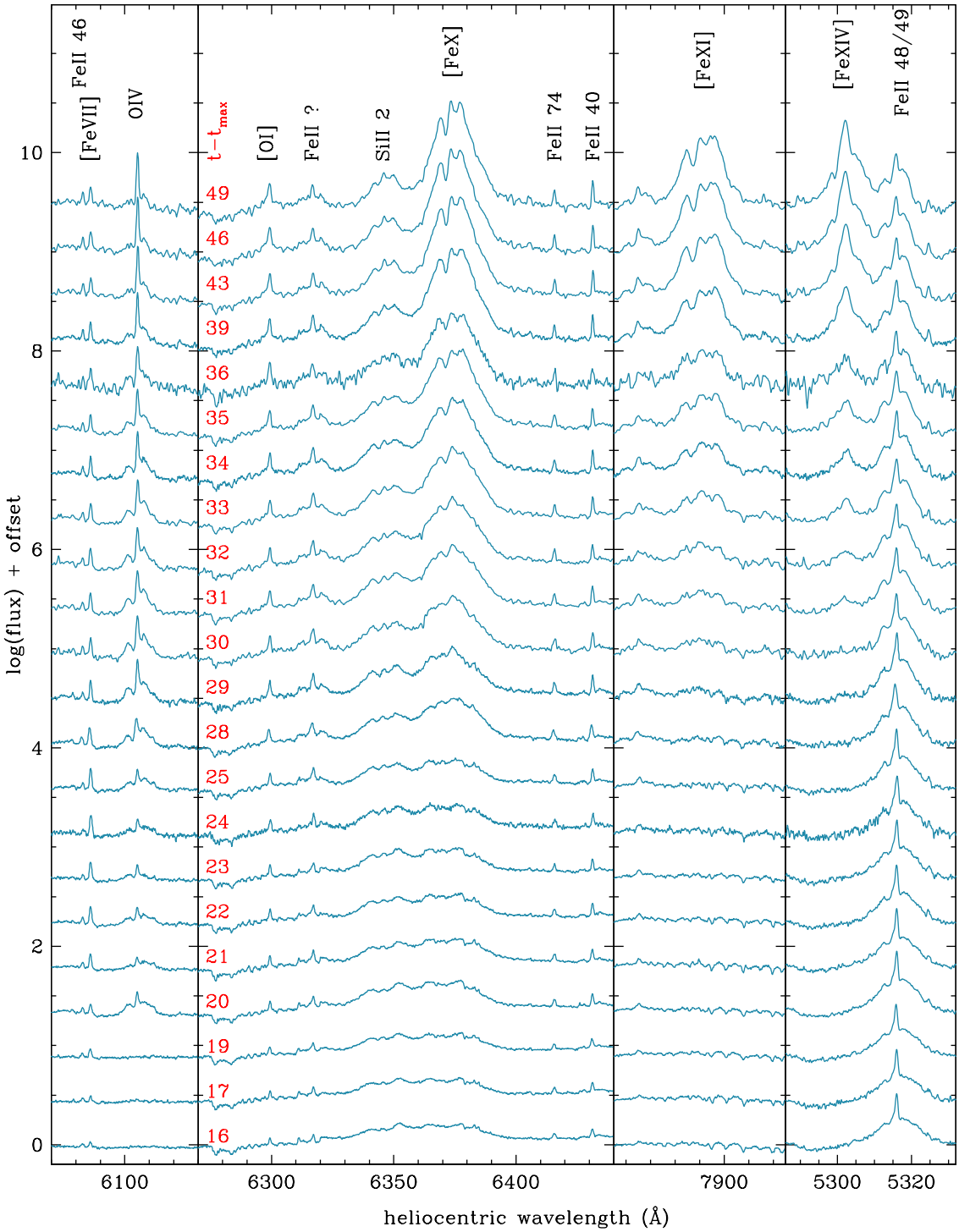

Figure 6: Evolution from day 16 to 102 of selected emission lines in our Echelle spectra of the 2021 outburst of RS Oph (cf Table 1). The $t - t_{\rm max}$ time from maximum (in days) is marked in red next to each spectrum.

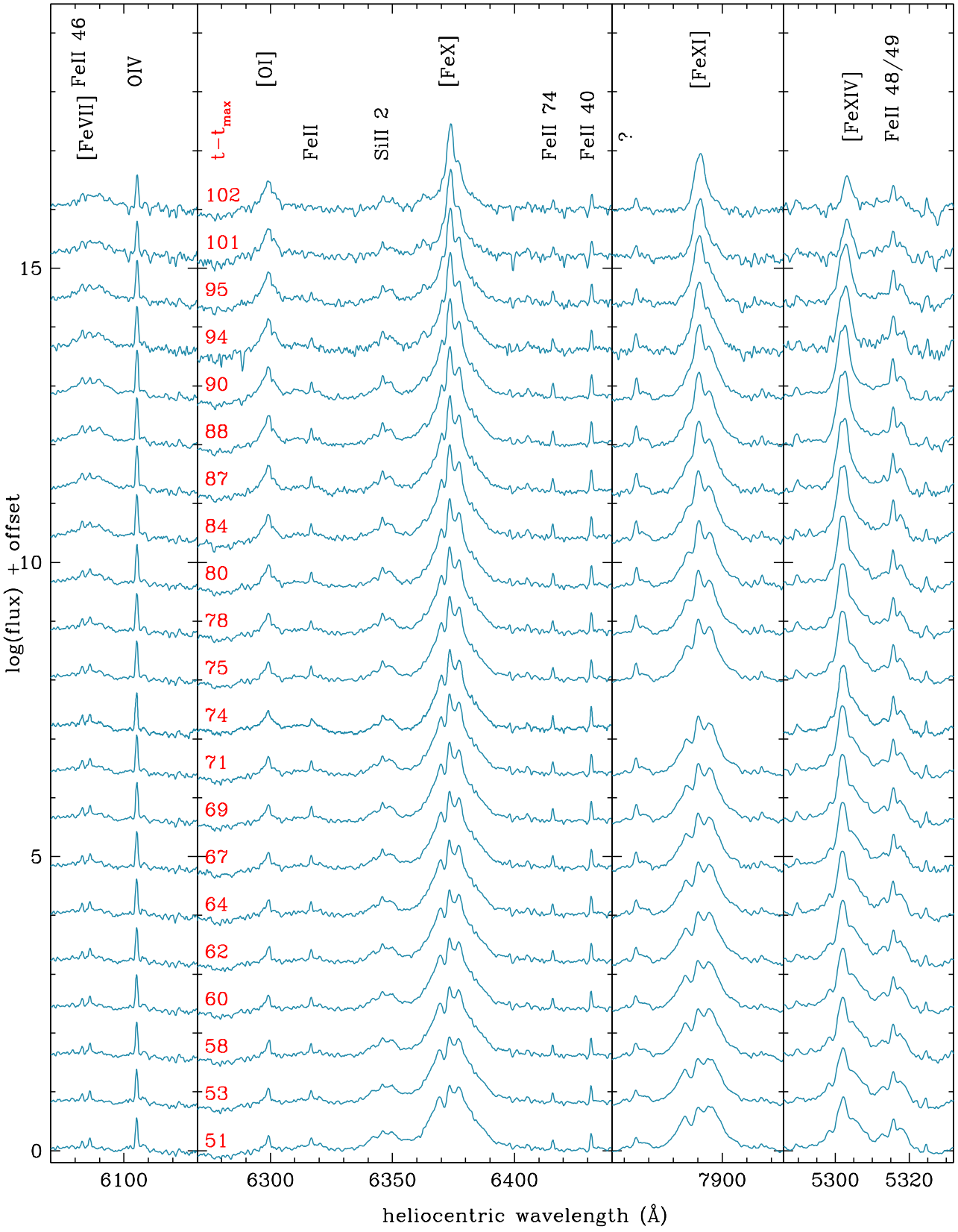

Figure 7: continues from Figure 6.

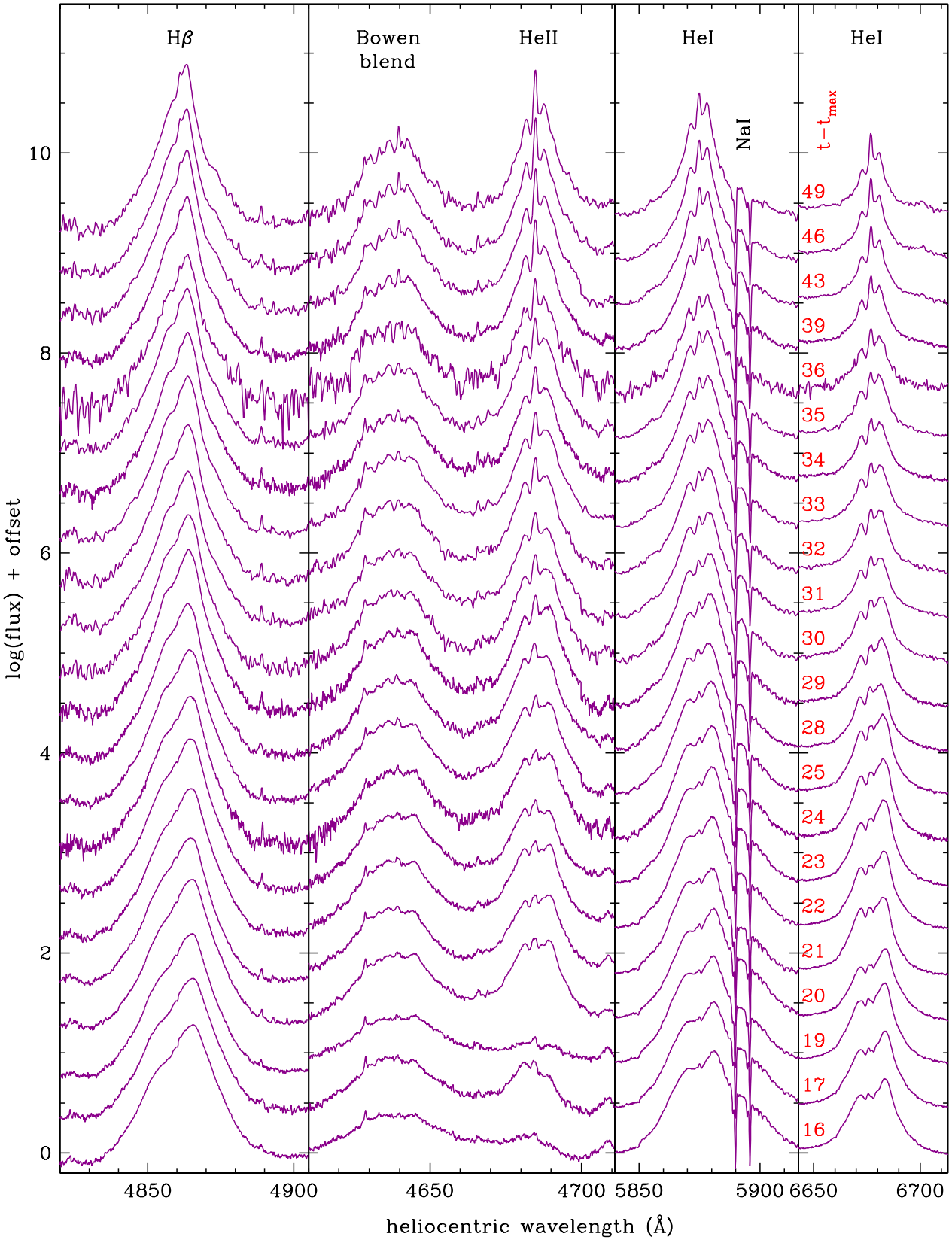

Figure 8: continues from Figure 6.

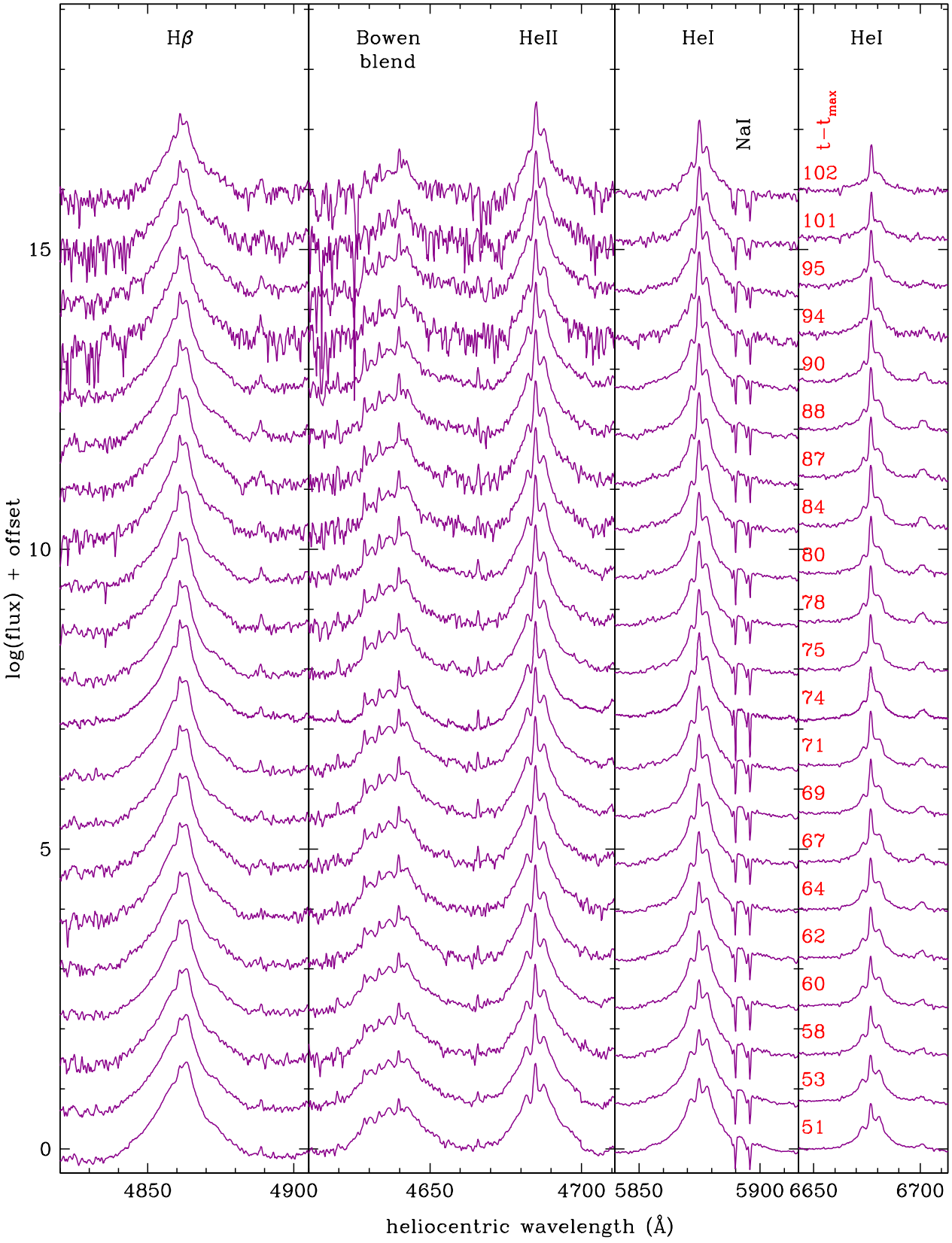

Figure 9: continues from Figure 6.

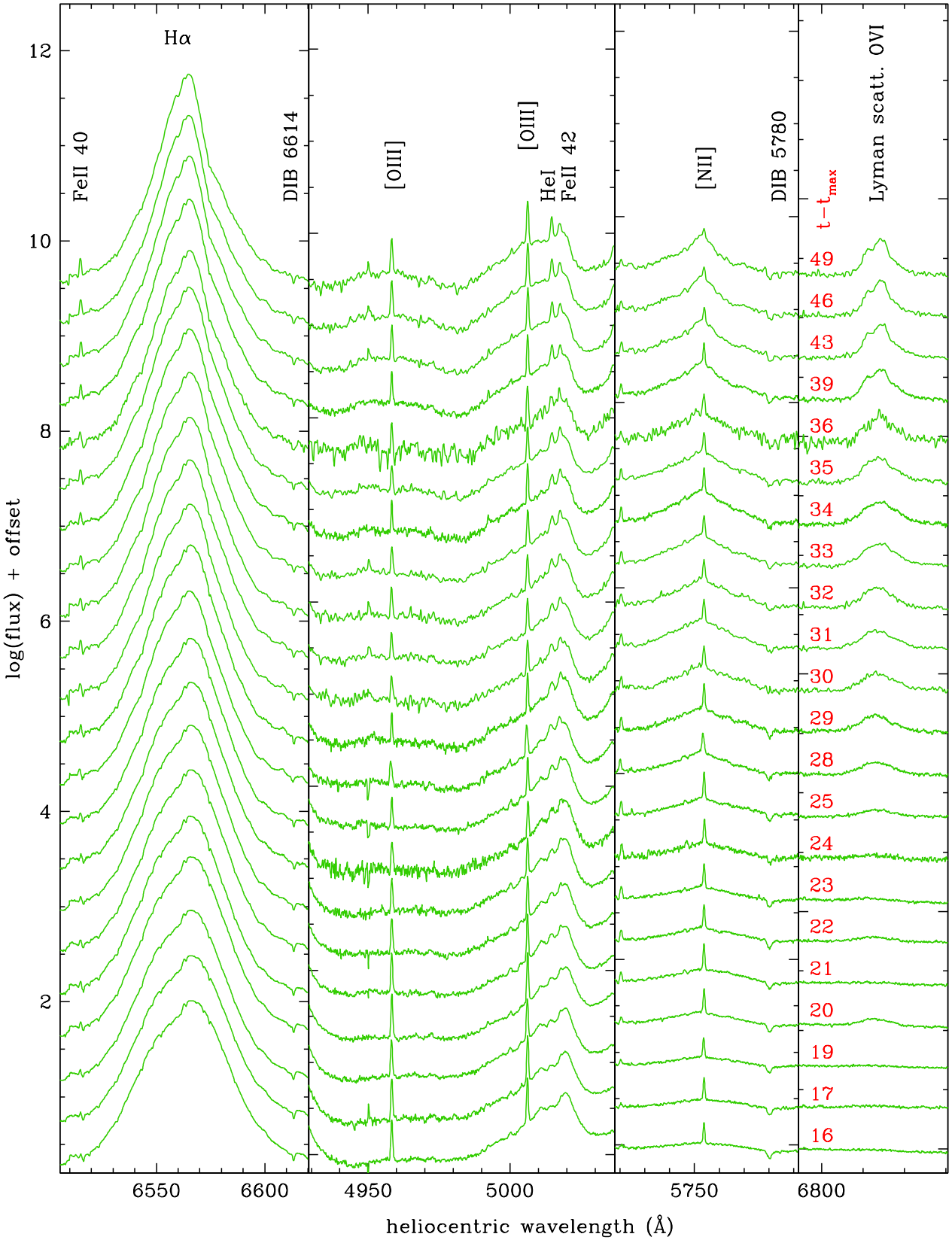

Figure 10: continues from Figure 6.

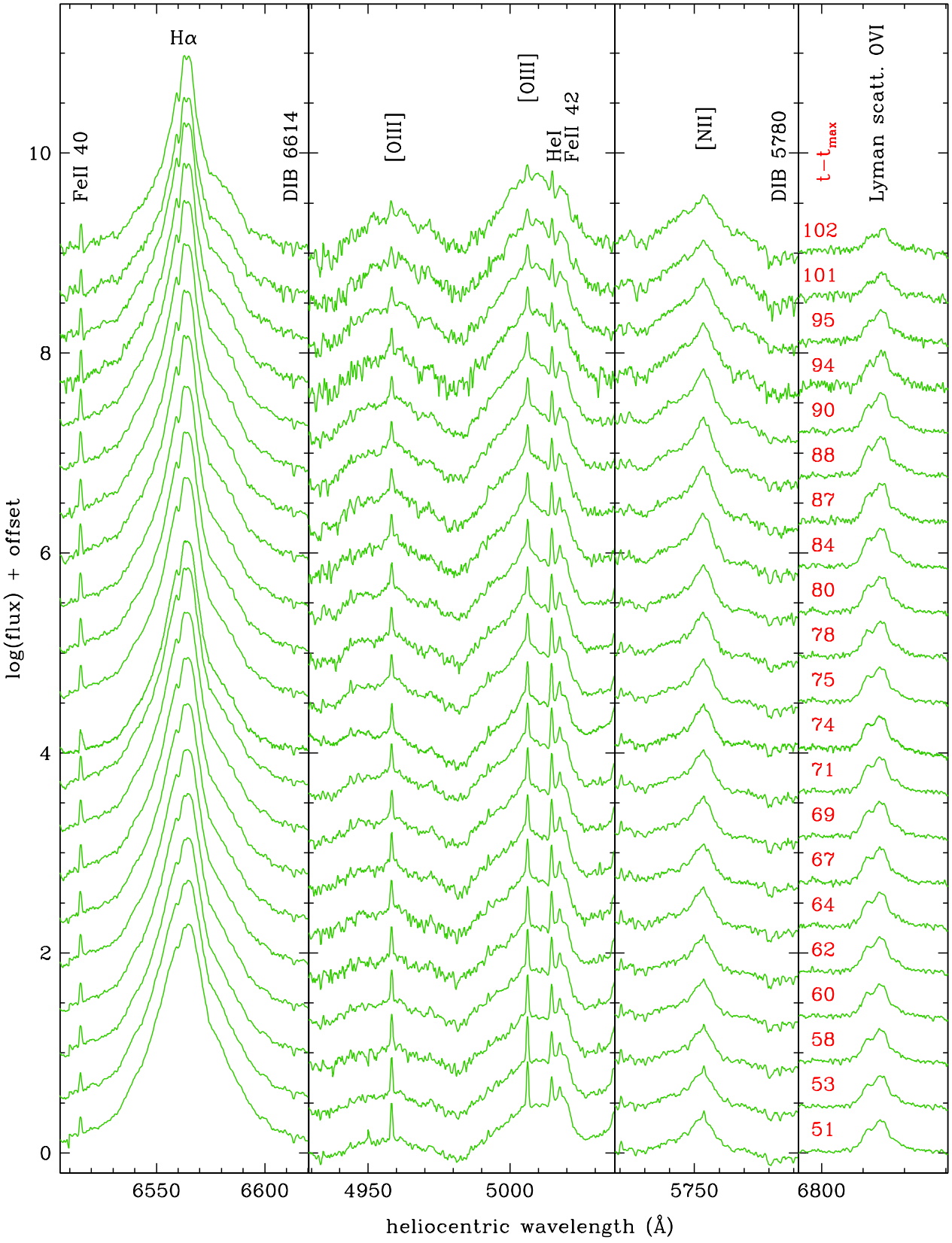

Figure 11: continues from Figure 6.

10. REFERENCES

Cheung C. C., Ciprini S., Johnson T. J., 2021a, ATel, 14834
Cheung C. C., Johnson T. J., Mereu I., et al., 2021b, ATel, 14845
Enoto T., Maehara H., Orio M., et al., 2021a, ATel, 14850
Enoto T., Orio M., Fabian A., et al., 2021b, ATel, 14864
Evans A., Bode M. F., O'Brien T. J., Darnley M. J., eds., 2008, RS Ophiuchi (2006) and the Recurrent Nova Phenomenon, ASPC, 401
Fajrin M., Imaduddin I., Malasan H. L., et al., 2021, ATel, 14909
Ferrigno C., Savchenko V., Bozzo E., et al., 2021, ATel, 14855
H.E.S.S. Collaboration, et al., 2022, arXiv:2202.08201
Luna G. J. M., Jimemez-Carrera R., Enoto T., et al., 2021, ATel, 14872
MAGIC Collaboration, et al., 2022, arXiv:2202.07681
Mikolajewska J., Aydi E., Buckley D., et al., 2021, ATel, 14852
Montez R., Luna G. J. M., Mukai K., et al. , 2021, arXiv:2110.04315
Munari U., Valisa P., 2021a, ATel, 14840
Munari U., Valisa P., 2021b, ATel, 14860
Munari U., Valisa P., 2021c, arXiv 2109.01101 (Paper I)
Munari U., Valisa P., Ochner P., 2021, ATel, 14895
Munari U., Valisa P., Dallaporta S., 2022, ATel, 15169
Munari U., Zwitter T., 2002, A&A 383, 188
Nikolov Y., Luna G. J. M., 2021, ATel, 14863
Orio M., Behar E., Drake J., et al. , 2021a, ATel, 14906
Orio M., Gendreau K., Pei S., et al., 2021b, ATel, 14926
Orio M., Gendreau K., Pei S., et al., 2021c, ATel, 14954
Page, K. L. 2021a, ATel, 14885
Page K. L., 2021b, ATel, 14894
Page K. L., Osborne J. P., Aydi E., 2021, ATel, 14848
Pei S., Orio M., Gendreau K., et al., 2021, ATel, 14901
Pizzuto A., Vandenbroucke J., Santander M., IceCube Collaboration, 2021, ATel, 14851
Ricra J., Vannini J., Baella N. O., 2021, ATel, 14972
Rout S. K., Srivastava M. K., Banerjee D. P. K., et al., 2021, ATel, 14882
Schmid, H.M. 1989, A&A 211, L31
Shidatsu M., Negoro H., Mihara T., et al., 2021, ATel, 14846
Shore S. N., Allen H., Bajer M., et al., 2021a, ATel, 14868
Shore S. N., Teyssier F., Thizy O., 2021b, ATel, 14881
Shore S. N., Teyssier F., Guarro J., et al., 2021c, ATel, 14883
Sokolovsky K., Aydi E., Chomiuk L., et al., 2021, ATel, 14886
Taguchi K., Ueta, T., Isogai, K., 2021a, ATel, 14838
Taguchi K., Maheara H., Isogai K., et al., 2021b, ATel, 14858
Wagner, S. J., HESS Collaboration, 2021a, ATel, 14844
Wagner, S. J., HESS Collaboration, 2021b, ATel, 14857
Williams D., O'Brien T., Woudt P., et al., 2021, ATel, 14849
Woodward C. E., Evans A., Banerjee D. P. K., et al., 2021a, ATel, 14866
Woodward C. E., Banerjee D. P. K., Evans A., et al., 2021b, ATel, 14910
Zamanov R. K., Stoyanov K. A., Kostov A., et al., 2021a, ATel, 14974
Zamanov R. K., Stoyanov K. A., Nikolov Y. M., et al., 2021b, arXiv:2109.11306
Zwitter T., Munari U., 2000, An introduction to analysis of spectra with IRAF, Univ. of Padova (2000iasd.book.....Z)